Available online at www.sciencedirect.com
ScienceDirect
Journal of Molecular Spectroscopy 00 (2012) 1–17
J Mol Spectrosc

Raman and infrared spectra of dimethyl ether ^{13}C-isotopologue ($CH_3O^{13}CH_3$) from a CCSD(T) potential energy surface

M. Carvajal*, O. Álvarez-Bajo

Dpto. Física Aplicada, Facultad de Ciencias Experimentales, Universidad de Huelva, 21071 Huelva, Spain

M. L. Senent**

Dpto. de Química y Física Teóricas, Instituto de Estructura de la Materia, IEM-C.S.I.C., Serrano 121, Madrid 28006, Spain

R. Domínguez-Gómez

Dpto. de Ingeniería Civil, Cátedra de Química, E.U.I.T. Obras Públicas, Universidad Politécnica de Madrid, Spain

M. Villa

Dpto. de Química, UAM-I Purísima y Michoacan, s/n, México D.F. 09340, Mexico

Abstract

So far, no experimental data of the infrared and Raman spectra of ^{13}C isotopologue of dimethyl ether is available. With the aim of providing some clues of its low-lying vibrational bands and with the hope of contributing in a next spectral analysis, a number of vibrational transition frequencies below 300 cm^{-1} of the infrared spectrum and around 400 cm^{-1} of the Raman spectrum have been predicted and their assignments were proposed. Calculations were carried out through an *ab initio* three dimensional potential energy surface based on a previously reported one for the most abundant dimethyl ether isotopologue (M. Villa, *et al.*, *J. Phys. Chem. A* 115 (2011) 13573). The potential function was vibrationally corrected and computed with a highly correlated CCSD(T) method involving the COC bending angle and the two large amplitude CH_3 internal rotation degrees of freedom. Also, the Hamiltonian parameters could represent a support for the spectral characterization of this species. Although the computed vibrational term values are expected to be very accurate, an empirical adjustment of the Hamiltonian has been performed with the purpose of anticipating some workable corrections to any possible divergence of the vibrational frequencies. Also, the symmetry breaking derived from the isotopic substitution of ^{13}C in the dimethyl ether was taken into account when the symmetrization procedure was applied.

Keywords: CH_3OCH_3, dimethyl ether, isotopologues, ab initio, infrared, Raman

1. Introduction

Molecular spectroscopy provides transition frequencies and line intensities necessary for the astronomical detection of molecular species. With these spectroscopic data, the spectral confusion of the surveys is being solved allowing

*E-mail: miguel.carvajal@dfa.uhu.es. Phone number: +34-959219792. Fax Number: +34-959219777.
**E-mail: senent@iem.cfmac.csic.es. Phone number: +34-915616800.

new molecular identifications. This requires the collaborative effort of spectroscopy and astronomical observation research groups.

In particular, the characterization of isotopologues is important from the astronomical point of view for determining the isotopic abundances in the *interstellar medium* (ISM). By comparing isotopic ratios in different ISM regions, some clues about the origin of astronomical objects and their molecules could be derived. For example, the D/H ratio was used to estimate the origin of Earth's water [1]. A similar study could be carried out by measuring the $^{12}C/^{13}C$ isotopic ratio of complex molecules, which will allow us to gain an insight into the formation mechanism of the molecular species. Although many isotopic varieties containing ^{13}C have been spectroscopically characterized to allow their astronomical detection (i.e. for C_4 [2], C_5 [3], methanol [4], methyl formate [5, 6], ethyl methyl ether [7]), the ^{13}C isotopologues of many other species cannot be identified in the ISM due to the lack of their spectral recordings. This is the case of dimethyl ether (DME).

As far as we know, experimental spectroscopic studies of DME in gas phase were carried out from 1957 [8], when its vibrational Raman spectrum was recorded, and from 1959 [9], when for the first time the microwave spectrum was used to characterize its molecular structure. Afterwards, a sequence of spectroscopic works was carried out. During the sixties, Fateley & Miller recorded the far infrared spectrum [10] and Blukis *et al.* used the MW spectrum (barely 10 lines) of the most abundant variety to determine the structure of six additional isotopologues, providing also its dipole moment [11]. The seventies were characterized by the beginning of its torsional splitting analysis. For the parent species CH_3OCH_3 (DME-h_6) and two deuterated species CH_3OCD_3 (DME-d_3) and CD_3OCD_3 (DME-d_6), Durig *et al.* [12] determined the torsional potential barrier height through the measurement of tens of lines (19-40 GHz) in the ground vibrational state (g.s.) and Groner & Durig [13] provided their Raman and far infrared spectra. Also, Lovas *et al.* measured and assigned 157 lines (9-112 GHz) in g.s. for DME-h_6 [14]. Moreover, in the seventies, the most abundant DME isotopologue was detected for the first time in the ISM. The discovery was carried out in the Orion nebula molecular cloud [15].

Later on, DME spectral analysis was revisited by Neustock *et al.* [16] with the measurement of 66 new lines (63-222 GHz) corresponding to the ground state (g.s.) of DME-h_6, and by Groner *et al.* [17] with the first extensive spectral recording (over 1100 lines in the frequency range of 94-544 GHz). This last analysis was performed by means of the ERHAM global analysis code [18]. Recently, three fundamental stretching bands were rotationally analyzed [19] and a new molecular structure was derived from MW measurement of some tens of lines (12-25 GHz) in g.s. for 17 isotopologues [20]. In 2009, Endres *et al.* measured 1600 lines (39 GHz -2.1 THz) in g.s. for DME-h6 and a global analysis was carried out with ERHAM [21].

Nevertheless, for a correct spectral analysis, a suitable theoretical model is needed specially when highly excited spectral lines have been recorded and their assignments are required. DME has a complex spectrum caused mainly by the two large-amplitude torsional modes which split the spectral lines into nine components since the full-dimensional potential energy surface (PES) shows nine equivalent minima. In 1995, Senent *et al.* anticipated the future spectroscopic requirements for the study of highly excited states of DME, determining the *ab initio* torsion-bending spectrum of CH_3OCH_3 and CD_3OCD_3 with Möller-Plesset theory and a double-ζ basis set [22, 23]. These works proved that to analyze transition lines involving higher excited torsional states than fundamentals the Fermi interaction between the torsional modes and the COC-bending mode is needed in the theoretical formalism [23]. Recently, a more accurate *ab initio* study of the infrared and Raman spectra of main isotopologue was made [24]. A new three dimensional potential energy surface was determined using highly correlated ab initio calculations (CCSD(T)) in order to predict the frequencies of overtones and combination bands corresponding to the torsional modes and the COC bending mode. Besides, a PES adjustment was performed to improve the accuracy of the transition frequencies. The potential surface was also verified through the analysis of the isotopologues DME-d_3 and DME-d_6 [25] for which previous experimental data were available [13]. In 1997, an approach for dealing with two-top molecules by means of an effective rotational Hamiltonian was thought up and applied to DME spectral analysis (ERHAM [18]). Since then, other different studies were carried out for the microwave spectral analysis of two unequivalent methyl top molecules as e.g. N-methylacetamide [26], methyl acetate [27], ethyl methyl ether [28], and the *ab initio* CCSD(T) study of infrared spectrum of ethyl methyl ether [29].

The present work is motivated by the relatively high abundance of DME in star-forming regions where highly excited rotational lines have been observed [30]. This fact makes us to expect that torsionally excited DME-h_6 and ^{13}C isotopologue of dimethyl ether $^{12}CH_3O^{13}CH_3$ (DME-^{13}C) should be observed in the ISM, as it occurs with other complex one torsional methyl top molecules such as methyl formate detected in Orion KL and W51 e2 clouds [5, 31].

The lack of spectral recordings for the torsional excited lines of DME-h_6 and for DME-^{13}C can explain why they have not been identified yet. However, their spectra are in the way of being solved (Private Communication. M. Koerber, C. Endres, S. Schlemmer, I. Kleiner) [32].

In this paper we report some theoretical frequencies corresponding to the infrared and Raman spectra of DME-^{13}C aiming to help forthcoming spectral analysis. In our theoretical model, a 3D vibrational Hamiltonian involving two large-amplitude motions relative to the two CH_3 internal rotors of the molecule and the COC bending mode is solved variationally. As it is shown in previous works, the COC bending mode needs to be explicitly considered as independent variable to obtain a suitable description of the lowest energy torsional states [23, 24]. The calculations are based on the *ab initio* CCSD(T) state-of-the-art PES and its adjustment given in Ref. [24]. The symmetrized basis set used for diagonalizing the Hamiltonian has been obtained by means of the symmetry projection method different to the textbook approach, as was explained in Refs.[33, 34].

This paper is organized as follows. In Section 2 the variational procedure is presented, providing some details about the 3D torsion-torsion-bending Hamiltonian and the determination of the *ab initio* PES and kinetic parameters. In Section 3 some symmetry considerations are dealt for the most abundant species and for DME-^{13}C. In Section 4, vibrational energy levels of DME-^{13}C are determined and shown. Finally, conclusions are presented in Section 5.

2. Computational details

Dimethyl ether is a non-rigid molecule with two strongly coupled equivalent methyl groups that also interact with the COC bending mode by means of a Fermi interaction. For this reason, it is necessary to consider these three vibrational modes altogether in our approach in order to obtain a suitable description of the lowest frequency range of the vibrational spectra. The vibrational term values were obtained by means of a variational procedure that includes a 3D torsion–torsion–bending Hamiltonian.

The potential energy surface and its molecular structure were calculated by CCSD(T) *ab initio* calculations in a previous paper devoted to the study of the most abundant isotopologue DME-h_6 [24]. In this work, the same procedure and PES is applied to interpret the DME-^{13}C properties by taking into account two facts: first, the loss of symmetry derived from the isotopic substitution of one ^{12}C atom by ^{13}C, and also that some of the parameters of the 3D-Hamiltonian are isotopically dependent and need to be recalculated. Some hints of the variational procedure are given below.

2.1. Effective torsion-torsion-bending Hamiltonian

DME two methyl top rotations are described by the torsional angles θ_1 and θ_2 while the COC bending angle is given by α. With these internal coordinates, a 3D torsion-torsion-bending Hamiltonian is built up as:

$$\hat{H}(\alpha,\theta_1,\theta_2) = -\sum_{\beta,\beta'} \frac{\partial}{\partial\beta} B_{\beta\beta'}(\alpha,\theta_1,\theta_2)\frac{\partial}{\partial\beta'} + V^{\mathrm{ef}}(\alpha,\theta_1,\theta_2) \tag{1}$$

where the effective potential energy surface V^{ef} represents the sum of three terms: the potential energy surface $V(\alpha,\theta_1,\theta_2)$, the *Podolsky pseudopotential* $V'(\alpha,\theta_1,\theta_2)$ and the zero point vibrational energy correction $V^{ZPVE}(\alpha,\theta_1,\theta_2)$. The subindexes β,β' run over the internal coordinates α,θ_1,θ_2. Whereas the Potential Energy Surface V is isotopically invariant, V', V^{ZPVE} and the kinetic matrix elements $B_{\beta\beta'}$, are functions of the nuclei masses of the molecule.

In Ref. [24], a very accurate Potential Energy Surface V was obtained from the total electronic energies of 126 molecular structures which were selected following energy and symmetry criteria. They were determined using Coupled Cluster theory with both single and double substitutions, including perturbatively the triple excitations (CCSD(T)) [35]. The augmented basis set aug-cc-pVTZ was employed in all the computations [36]. For each structure, defined for selected values of the three independent coordinates, the remaining eighteen internal coordinates were optimized at the CCSD level. In addition, as an artificial break of the C_{3v} symmetry of the tops appears during the optimization process, the torsional coordinates were carefully defined in order to preserve the threefold symmetry [24]. Definitions of the independent coordinates are given in Ref. [24, 37]. There, the torsional coordinates are defined as linear combination of three COCH dihedral angles and the bending coordinate is identified with the COC curvilinear internal coordinate.

The pseudopotential V' and the kinetic parameters $B_{\beta\beta'}$ were obtained for each 126 CCSD geometries through the MATRIZG subroutine implemented in ENEDIM code [38] and later on, they were fitted to symmetry adapted functions (see below). How these subroutines work is detailed in Ref. [39].

For DME-^{13}C, the ZPVE correction V^{ZPVE} has been determined in present paper from the MP2/aug-cc-pVTZ harmonic frequecies ω_i of the remaining vibrational modes:

$$V^{ZPVE} = \sum_{i=n+1}^{3N-6} \frac{\omega_i}{2} \tag{2}$$

where the sum neglects the two torsional and the COC bending modes ($n = 3$) and runs over the total number of vibrational modes in the molecule ($3N - 6$).

2.2. Torsion-torsion-bending basis set

DME 3D torsion-torsion-bending Hamiltonian [24] is solved variationally with a basis set expressed in a symmetrized form made up of a product of two torsional free rotor wavefunctions [40] and the COC bending harmonic oscillator wavefunction.

For a molecule with one CH_3 internal rotor with a molecular symmetry group $C_{3v}(M)$, the torsional wavefunctions are given by

$$|v_t, \sigma\rangle = \sum_{k=-k_{max}}^{k_{max}} A_k^{v_t,\sigma} e^{i(3k+\sigma)\gamma} \tag{3}$$

where γ is the torsional angle, k runs from $-k_{max}$ to $+k_{max}$, v_t is the torsional quantum number and σ provides the symmetry of the torsional state. When $\sigma = 0$ the torsional state carry A symmetry (either A_1 or A_2 irreducible representations) and whether $\sigma = \pm 1$, the torsional state bears the E symmetry irreducible representation [41].

For the dimethyl ether, two internal CH_3 rotors with torsional angles θ_1 and θ_2 should be involved in the calculations. Therefore, the torsional basis set for the internal rotors of DME is given by:

$$\phi^{(\mathrm{tor})} = e^{i(3k_a+\sigma_a)\theta_1} e^{i(3k_b+\sigma_b)\theta_2} \qquad \sigma_i = 0, \pm 1 \tag{4}$$

where σ_a and σ_b will provide us the symmetries of the torsional states

$$\langle \theta_1, \theta_2 | v_t, v_t', \sigma_a, \sigma_b \rangle = \sum_{k_a,k_b=-k_{max}}^{k_{max}} C_{k_a,k_b}^{v_t,v_t',\sigma_a,\sigma_b} e^{i(3k_a+\sigma_a)\theta_1} e^{i(3k_b+\sigma_b)\theta_2} \tag{5}$$

in the spectroscopic notation AA, AE, EA, and EE for (σ_a, σ_b) equal to $(0, 0)$, $(0, \pm 1)$, $(\pm 1, 0)$, $(\pm 1, \pm 1)$ respectively. The torsional quantum numbers are given by the labels v_t and v_t'. Also, the wavefunctions could be written as a double trigonometric series according to the symmetry of the torsional states [23, 42].

The extension of the 2D torsional basis set to a 3D torsion-torsion-bending basis set is obtained straightforwardly by the product of the COC bending harmonic wavefunction $\Phi_{n_b}^{(h.o.)}(\alpha)$ to the torsional states (5):

$$\langle \theta_1, \theta_2, \alpha | v_t, v_t', n_b; \Gamma_{tb} \rangle = \langle \theta_1, \theta_2 | v_t, v_t', \sigma_a, \sigma_b \rangle \, \Phi_{n_b}^{(h.o.)}(\alpha) \tag{6}$$

where n_b is the harmonic COC bending quantum number and Γ_{tb} is the symmetry of the state. The harmonic wavefunction for the COC bending is characterized as follows

$$\langle \alpha | n_b \rangle = \Phi_{n_b}^{(h.o.)}(\alpha) = \mathcal{N}_{n_b} e^{-\frac{\beta^2\alpha^2}{2}} H_{n_b}(\beta\alpha) \quad ; \quad \beta^2 = \sqrt{\frac{A_{200}}{C_{\alpha\alpha}^{200}}} \tag{7}$$

where β is obtained by the parameters of the zeroth-order harmonic Hamiltonian of the COC bending mode: the kinetic parameter $C_{\alpha\alpha}^{200}$, with information of COC bending reduced mass, and the pure bending second-order force constant A_{200} (see below). $\mathcal{N}_{n_b}$ is the normalization constant and H_{n_b} are Hermite polynomials. The COC bending states can be dealt in second quantization.

2.3. Adjustment of the 3D potential energy surface

The *ab initio* potential surface was used in the calculation of the DME vibrational term values. Although pure *ab initio* results are very accurate, computed energies were slightly deviated from the experimental ones [24] (3 cm^{-1} the torsional fundamentals and 8 cm^{-1} the bending fundamental for DME-h_6). In our previous paper, we have performed an empirical adjustment of the PES in order to understand the origin of this deviation. We concluded that these small errors came mainly from two causes, one reflected in the overestimation of the pure COC bending energies and another observed in the energy gap between the torsional antigearing and gearing modes that is extremely difficult to reproduce well from pure *ab initio* calculations given the artificial loss of symmetry derived from the optimization processes.

The first source of these small errors was caused by the definition of the bending coordinate. In our 3D model, the COC bending coordinate is identified with one internal coordinate, the COC in-plane angle α. Thus, we have introduced an error since the bending COC normal coordinate is not 100% the COC bending angle but also has a contribution of the other internal coordinates lying on the molecular plane. Therefore, in order to correct the COC bending energy levels, a new definition of the COC bending coordinate that weights the α contribution in the normal coordinate should be carried out:

$$\alpha' = \alpha\,(1 + Factor/100)\ , \tag{8}$$

and should be substituted in the Hamiltonian (1) besides changing the kinetic matrix parameter $B_{\alpha\alpha}$ by:

$$B'_{\alpha\alpha} = B_{\alpha\alpha}\,(1 - Factor/100)\ . \tag{9}$$

Actually, the new coordinate α', and hence the $Factor$ value in its definition, is obtained after adjusting the PES to the available experimental data [24, 25].

The second source of error came from the B_{011} parameter of the potential energy surface mainly responsible of the energy differences between the gearing and antigearing torsional motions. The *ab initio* value of the parameter resulted in pushing up the antigearing torsional energy level while the gearing torsional energy levels were pushed down. A slight change of the B_{011} parameter value was required in order to correct the gap differences between the gearing and antigearing torsional term values.

3. Symmetry considerations

Symmetry properties for a molecular system with two equivalent tops, as DME-h_6, and with two unequivalent tops, as DME-^{13}C, were derived long time ago (see e.g. Refs. [13, 42, 43]). However, in this paper a symmetry projection different to a textbook approach is carried out. This is based on a very efficient formalism that was recently applied to the study of the molecular vibrational and rovibrational structure [33, 34]. Besides, with the aim of working with a number of DME isotopologues, the consideration of the correlation tables among their molecular symmetry (MS) groups will allow us to interrelate their symmetry adapted basis sets.

The symmetrization procedure of a selected basis set for both main and ^{13}C species is carried out by the *eigenfunction method* [44] as described in Refs. [33, 34]. General features and steps to follow are given below. A linear combination of the symmetry group elements is built from some equivalence classes of the group. This linear combination is appropriately chosen when the eigenvalues of its diagonalization for the basis set distinguishes each one of the irreducible representations of the molecular symmetry group. This linear combination is called Complete Set of Commuting Operators of type I (CSCO-I). If some irreducible representations are degenerate, the last step is repeated but for a subgroup of the molecular symmetry group, in order to distinguish each component of the degenerate irreducible representation. The linear combination of both CSCO for the molecular symmetry group and the subgroup is called CSCO of type II (CSCO-II). Therefore, the diagonalization of CSCO-II should provide eigenvalues that distinguish the irreducible representations and each of their components.

The hints for the building of the CSCO-I and CSCO-II are given by the λ tables [33, 34] constructed from the character tables of the molecular symmetry group and the chosen subgroup through the formula [44]

$$\lambda_i^{\Gamma} = \frac{|K_i|\chi_i^{(\Gamma)*}}{n_{\Gamma}}, \tag{10}$$

where $|K_i|$ stands for the number of elements belonging to the i-th class, n_Γ corresponds to the dimension of the Γ-th irreducible representation, and $\chi_i^{(\Gamma)}$ is its character. Consequently, the eigenvalues assigned to each irreducible representation and their components can be known a priori through the character tables of the molecular symmetry group and the selected subgroup. Hence, the diagonalization of CSCO-II for the chosen basis set is carried out in order to obtain the eigenvectors, i.e., the symmetry adapted basis set.

Because we are interested in the torsion-torsion-bending degrees of freedom for DME, we will not deal with the rotational degrees of freedom here. In case that the global rotation is involved in the study, the symmetrized rotational basis set can be obtained from diagonalizing the CSCO-II operator with the symmetric-top rotational basis set. For that, the equivalent rotations [43] should be sought only for each symmetry element involved in the CSCO-II. Our symmetrized rotational basis sets are the same than those given in Ref. [27]. In order to study the microwave spectrum of a two-top molecule, a *complete* basis set of torsion-torsion-bending wavefunctions coupled with rotational functions should be used to diagonalize the CSCO-II that provides us the *complete* symmetry adapted basis set.

The COC bending mode has a totally symmetric representation. Therefore, the symmetry of the torsion-torsion-bending wavefunctions only depends on the transformation of the torsion-torsion wavefunction (4) under the symmetry operations. In order to obtain a symmetry adapted basis set, the CSCO-II operator should be diagonalized in a subspace of the torsional basis set. The torsional basis set subspace is chosen for each set of possible values of (σ_a, σ_b) in order that their torsional functions intertransform under the symmetry operations. Hence, the subspace, for a given set (σ_a, σ_b), is the following:

$$\begin{aligned}
\phi_1^{(\mathrm{tor})} &= |k_a, k_b\rangle \\
&= e^{i(3k_a+\sigma_a)\theta_1} e^{i(3k_b+\sigma_b)\theta_2} \\
\phi_2^{(\mathrm{tor})} &= |k_b, k_a\rangle \\
&= e^{i(3k_b+\sigma_b)\theta_1} e^{i(3k_a+\sigma_a)\theta_2} \\
\phi_3^{(\mathrm{tor})} &= |-k_a, -k_b\rangle \\
&= e^{-i(3k_a+\sigma_a)\theta_1} e^{-i(3k_b+\sigma_b)\theta_2} \\
\phi_4^{(\mathrm{tor})} &= |-k_b, -k_a\rangle \\
&= e^{-i(3k_b+\sigma_b)\theta_1} e^{-i(3k_a+\sigma_a)\theta_2}
\end{aligned} \tag{11}$$

3.1. $\mathcal{G}_{36}$ symmetry

DME-h_6 has a molecular symmetry group $\mathcal{G}_{36}$ [42] and, at the equilibrium, a molecular point group C_{2v}, where this latter is a subgroup of the former one. In Tables 1 and 2, character tables corresponding to the molecular symmetry groups $\mathcal{G}_{36}$ and $C_{2v}(M)$ are shown with their symmetry elements grouped as equivalence classes. The labeling of the atom nuclei is given in Fig. 1.

The CSCO-II is chosen as a linear combination of symmetry elements involved in the chain $\mathcal{G}_{36} \supset C_{2v}(M)$ in order to distinguish among irreducible representations and their components. This operator could be chosen as

$$\hat{C}_{II} = K_3 + 3\,K_7 + 2(K_2' + 3K_4') \tag{12}$$

where K_3 and K_7 are equivalence classes of $\mathcal{G}_{36}$ (see Table 1), and K_2' and K_4' are equivalence classes of $C_{2v}(M)$ (see Table 2). The sum of all the symmetry elements belonging to the classes in Eq. (12) produces the CSCO-II. The eigenvalues of Eq. (12) are given in Table 3 and provide the irreducible representations of $\mathcal{G}_{36}$ and distinguish their components through the irreducible representations of $C_{2v}(M)$. In this table the subduction $\mathcal{G}_{36} \downarrow C_{2v}(M)$ is also presented. With the subspace (11), for a given set (σ_a, σ_b), the CSCO-II is diagonalized and the eigenvectors are obtained (see Table 4). In fact, the torsional symmetry adapted basis sets are obtained through a linear combination of the result of Table 4 for a given symmetry after summing them over k_a and k_b values from $-k_{max}$ to $+k_{max}$ (see Eq. (5)).

For $\mathcal{G}_{36}$ molecule, the symmetry of the molecular dipole moment in the laboratory axis system $\Gamma(\mu_A) = A_3$ but the infrared transitions, corresponding to the Q branches of c-type bands are given by the symmetry of the c-component of the molecular dipole moment in the molecular fixed axis system $\Gamma(\mu_c) = A_2$ [24].

According to the Born-Oppenheimer approximation, the PES is the same for all DME isotopologues. That means that V is totally symmetric for the symmetry transformations of the $\mathcal{G}_{36}$ group. Therefore, the 3D-PES is expressed as:

$$\begin{aligned} V(\alpha,\theta_1,\theta_2) &= \sum_{M=0}^{4}\sum_{N=0}^{2}\sum_{L=0}^{2} A_{MNL}\alpha^M(\cos 3N\theta_1 \cos 3L\theta_2) \\ &+ \sum_{M=0} B_{M11}\alpha^M(\sin 3\theta_1 \sin 3\theta_2) \quad . \end{aligned} \tag{13}$$

3.2. $\mathcal{G}_{18}$ symmetry

The molecular symmetry group of its ^{13}C isotopologue is reduced to $\mathcal{G}_{18}$ while, at the equilibrium, its point group is reduced to C_s. In Refs. [26] and [27], symmetry discussions are carried out for the microwave spectral analysis of a two-top molecule with $\mathcal{G}_{18}$ symmetry. The equivalence classes are given in Table 5 according to Ref. [26].

After considering the case of DME-h$_6$, the simple way to tackle the symmetrization is through the subduction of $\mathcal{G}_{36}$ to $\mathcal{G}_{18}$ for obtaining the irreducible representations of DME-^{13}C and the subduction $C_{2v}(M)$ to $C_s(M)$ to distinguish the components of each degenerate irreducible representation of $\mathcal{G}_{18}$. In Table 6, the subduction from $\mathcal{G}_{36}$ to $\mathcal{G}_{18}$ is provided by showing the irreducible representations of $\mathcal{G}_{18}$ for each set (σ_a,σ_b). Thereby, the symmetry adapted basis of the torsional wavefunctions of DME-^{13}C can be obtained from the result given in Table 4 but taking into account the symmetry of $\mathcal{G}_{18}$ given in Table 6. The components of the degenerate irreducible representations of $\mathcal{G}_{18}$ are distinguished with the symmetry group $C_s(M)$. Therefore, the following subduction $\mathcal{G}_{18}\downarrow C_s(M)$, referred in Table 7, will provide us the components of the degenerate irreducible representations which are characterized by the values either $+1$ or -1 of σ_a and σ_b. The character table of $C_s(M)$ is presented in Table 8.

For $\mathcal{G}_{18}$, the symmetry of the molecular dipole moment in the laboratory axis system $\Gamma(\mu_A) = A_2$ but the infrared transitions, corresponding to the Q branches of c-type bands are given by the symmetry of the c-component of the molecular dipole moment in the molecular fixed axis system $\Gamma(\mu_c) = A_2$.

For DME-^{13}, due to the isotopic substitution of ^{13}C in DME, the mass-dependent potential functions V' and V^{ZPVE} have the same mathematical expression than V in Eq. (13) although they are totally symmetric respect to the symmetry transformations of $\mathcal{G}_{18}$ group. Hence, the effective PES V^{ef} is also expanded as in Eq. (13) and, as it is the sum of V, V' and V^{ZPVE}, it will bear the irreducible representation A_1 in the $\mathcal{G}_{18}$ molecular symmetry group and not of $\mathcal{G}_{36}$ group. As happens to the potential terms, the kinetic matrix elements also depend on the nuclei masses and therefore they are given as an expansion of the internal coordinates:

$$\begin{aligned} B_{\beta\beta'}(\alpha,\theta_1,\theta_2) &= \sum_{M=0}^{4}\sum_{N=0}^{2}\sum_{L=0}^{2} C^{MNL}_{\beta\beta'}\alpha^M(\cos 3N\theta_1 \cos 3L\theta_2) \\ &+ \sum_{M=0}^{4} S^{M11}_{\beta\beta'}\alpha^M(\sin 3\theta_1 \sin 3\theta_2) \quad , \end{aligned} \tag{14}$$

which will be totally symmetric respect to the $\mathcal{G}_{18}$ symmetry elements.

4. Application to ^{13}C-dimethyl ether

The torsional-bending energies of DME-^{13}C are obtained variationally. The *ab initio* PES $V(\alpha,\theta_1,\theta_2)$ of the Hamiltonian (1) was the same used for DME-h$_6$ [24]. For the DME-^{13}C, besides the obvious change of mass, some molecular structural variations are caused by the carbon substitution. The more evident is given by the transformation of a two equivalent methyl tops molecule to a two unequivalent tops one. As a consequence, the isotopic substitution effect is expressed mathematically by the expansion coefficients changes of the pseudopotential V' and the zero-point vibrational energy correction V^{ZPVE}, which cause the change of the effective potential expansion. Although changes in the effective potential expansion coefficients, defined as in Eq. (13), are very small, they are significative when an interchange of the subindexes of the potential expansion coefficients are carried out:

$$A_{MNL} \neq A_{MLN} \text{ when } N \neq L\,. \tag{15}$$

Therefore, for ^{13}C species, the potential term V is totally symmetric with respect to the $\mathcal{G}_{36}$ symmetry group whereas V' and V^{ZPVE} are totally symmetric with respect to the $\mathcal{G}_{18}$ group. Then, the effective potential V^{ef} transforms as totally symmetric representation of $\mathcal{G}_{18}$. The symmetry loss of the effective potential and the kinetic parameters, caused by the isotopic substitution, is perceptible in the coefficients of Table 9 and Table 10. In Table 9, the effective potential parameters are presented as they are defined in Eq. (13) and the isotopic substitution is noted in the fifth decimal of their coefficients. In Table 10, the more significant kinetic parameters are shown for DME-^{13}C according to Eq. (14). In fact, in Tables 9 and 10 the parameters presented are not the obtained with pure *ab initio* calculations but considering the corrections set out in Ref. [24] and detailed in Subsection 2.3. These corrections come from the new definition of the bending COC coordinate α' (8), which concerns to all the parameters through their dependence on the bending COC angle α, and from a further adjustment of B_{011} (see Eq. (13)). As there is no available experimental data for DME-^{13}C, it is assumed that the PES adjustment of DME-h$_6$ [24] could closely work in the present DME-^{13}C study. Therefore, the same adjusted effective potential function and kinetic term given in Ref. [24] were used in this work but considering the correction of the α coordinate for the DME-^{13}C and the geometrical changes derived from the isotopic substitution, i.e. in V', V^{ZPVE} and the kinetic matrix elements $B_{\beta\beta'}$. Hence, according to the contribution of adjustment of the COC angle α to the bending normal coordinate for DME-h$_6$, the bending angle correction of DME-^{13}C was also given by $Factor = 1.954$ in Eq. (8) whereas B_{011} was changed from the pure CCSD(T) value of -15.899 cm^{-1} to -2.899 cm^{-1} (see Table 9).

For the diagonalization of the Hamiltonian matrix, the torsional-bending basis set (6) was symmetrized as it has been explained in Section 3. The dimension of the Hamiltonian matrix is determined by the chosen value of k_{max} in Eq. (5) and the maximum quantum number n_b^{max} for the bending harmonic functions (7). High values of k_{max} and n_b^{max} guarantee the convergence of higher excited torsional-bending energies. In this work, the convergence of the transition frequencies among lowest excited states was reached up to their third decimals when $k_{max} = 22$ and $n_b^{max} = 13$, as was observed in Ref. [25].

In Tables 11 and 12, the computed frequencies of some low-lying transitions are presented for the infrared and Raman spectra, respectively. Under column *CCSD(T)* of former tables, the frequencies calculated with a pure *ab initio* CCSD(T)/aug-cc-pVTZ level of theory, with no further corrections, are given. Although they are expected accurate we do not dismiss some small divergences with respect to the *true* values. In order to delimit the *true* values of the transition frequencies, since there is no available experimental data to compare with our calculations, we have thought necessary to provide an alternative result coming from the parameters of Tables 9 and 10, i.e., obtained from the empirically adjusted *ab initio* PES (see Subsection 2.3). Their calculated frequencies are presented under the column marked by *Adjusted* of which we would expect that the possible existing divergence could be corrected. In Tables 11 and 12, we have classified the transition lines by symmetry besides proposing for them an assignment. The symmetry labeling characterizes the splitting caused by the two large-amplitude unequivalent tops.

We should remark some of the effects of the adjustment in the vibrational energies (see Tables 11 and 12). For example, on one hand, the bending angle correction concerns the pure COC bending energy level (0 0 1) by shifting its value from 418.5 cm^{-1} to 409.2 cm^{-1}. On the other hand, the effect of decreasing the absolute value of B_{011} caused that the energy gap drop between the gearing torsional state (1 0 0) and the antigearing torsional state (0 1 0) from a difference around 46 cm^{-1} to 41 cm^{-1}. It is expected that the frequency corrections are going in the right direction after being proven previously in Refs. [24, 25].

Also, it is interesting to highlight that for $\mathcal{G}_{36}$ DME species, the transition (1 0 0) $\rightarrow$ (0 0 0) (g.s.) is forbidden for both the infrared and Raman spectra. The torsional state (1 0 0) has A_3 symmetry in the $\mathcal{G}_{36}$ symmetry group while, e.g., in the infrared spectrum the symmetry of the c-component of the dipole moment is $\Gamma(\mu_c) = A_2$. For DME-^{13}C, this band can be observed in the infrared spectrum. The state (1 0 0) has A_2 symmetry in the $\mathcal{G}_{18}$ molecular symmetry group and according to $\Gamma(\mu_c)$, the infrared transition (1 0 0) $\rightarrow$ (0 0 0) (g.s.) is allowed.

This fact is very important in order to provide some information of the energy term value of (1 0 0) of main species, which can only be observed in less intense transitions when some combinations bands are involved. A first recording of the DME-^{13}C is longed to verify the *ab initio* PES of Ref. [24] when adjusted for ^{13}C-isotopologue and to resolve the energy term value of (1 0 0) of parent species through the *ab initio* PES.

5. Summary and conclusions

For first time, infrared and Raman low-lying transition frequencies have been computed for the DME-^{13}C. An *ab initio* three dimensional potential energy surface calculated with a highly correlated method for DME-h_6 [24] was vibrationally corrected and expanded in terms of the internal coordinates describing the COC bending and the two large-amplitude CH_3 internal rotation degrees of freedom. The vibrational term values were computed variationally after an appropriate symmetrization of the wavefunctions. Besides, according to previous infrared and Raman analysis of the main isotopologue [24] and of two deuterated species [25], an empirical adjustment of the *ab initio* 3D-PES was carried out in order to understand the possible small deviations between calculations and their *true* data.

In the infrared spectrum some allowed vibrational transitions below 300 cm^{-1} were presented and, for the Raman, some of those around 400 cm^{-1}. In total, 85 transition frequencies were predicted with a very good accuracy, as was proven in Refs. [24, 25]. The splittings caused by the torsional modes have also been resolved for each vibrational transition according to the standards of highly correlated *ab initio* calculations.

Due to no experimental frequencies have been recorded for the DME-^{13}C yet, these accurate calculations of the vibrational band positions could be useful whether measurements of the infrared and Raman spectra were carried out. Also, the calculated Hamiltonian parameters represent a good starting support for the spectral analysis in the microwave range and to characterize DME-^{13}C for astronomical purposes.

Acknowledgements

This work has been partially supported by European regional development funds (FEDER) under Junta de Andalucía project P07-FQM-03014, by the Spanish Government through grants AYA2008-00446 (Plan Nacional I+D+I (2004-2007)) and FIS2011-28738-C02-02, and computing resources of CESGA. The authors acknowledge to Prof. Renato Lemus his very valuable comments related to the symmetrization procedure and also thank to Prof. Jon T. Hougen and Prof. Isabelle Kleiner for their discussions during the work.

References

[1] P. Hartogh, D. C. Lis, D. Bockelée-Morvan, M. de Val-Borro, N. Biver, M. Küppers, M. Emprechtinger, E. A. Bergin, J. Crovisier, M. Rengel, R. Moreno, S. Szutowicz, G. A. Blake, Nature 478 (2011) 218–220.
[2] H. Masso, M. L. Senent, P. Rosmus, M. Hochlaf, J. Chem. Phys. 124 (2006) 234304.
[3] H. Masso, V. Veryazov, P. A. Malmqvist, B. Roos, M. Senent, J. Chem. Phys. 127 (2007) 154318.
[4] L.-H. Xu, M. Walsh, R. Lees, J. Mol. Spectr. 179 (1996) 269–281.
[5] M. Carvajal, L. Margulès, B. Tercero, K. Demyk, I. Kleiner, J. C. Guillemin, V. Lattanzi, A. Walters, J. Demaison, G. Wlodarczak, T. R. Huet, H. Mollendal, V. V. Ilyushin, J. Cernicharo, A&A 500 (2009) 1109–1118.
[6] M. Carvajal, I. Kleiner, J. Demaison, The Astrophysical J. Supp. Ser. 190 (2010) 315–321.
[7] M. L. Senent, R. Ruiz, M. Villa, R. Domínguez-Gómez, Chem. Phys. 368 (2010) 87–92.
[8] R. C. Taylor, G. L. Vidale, J. Chem. Phys. 26 (1957) 122–123.
[9] P. H. Kasai, R. J. Myers, J. Chem. Phys. 30 (1959) 1096.
[10] W. G. Fateley, F. A. Miller, Spectrochim. Acta 18 (1962) 977–993.
[11] U. Blukis, P. H. Kasai, R. J. Myers, J. Chem. Phys. 38 (1963) 2753–2760.
[12] J. R. Durig, Y. S. Li, P. Groner, J. Mol. Spectrosc. 62 (1976) 159–174.
[13] P. Groner, J. R. Durig, J. Chem. Phys. 66 (1977) 1856.
[14] F. J. Lovas, H. Lutz, H. Dreizler, J. Phys. Chem. Ref. Data 8 (1979) 1051.
[15] L. E. Snyder, D. Buhl, P. R. Schwartz, F. O. Clark, D. R. Johnson, F. J. Lovas, P. T. Giguere, Astrophys. J. 191 (1974) L79–L82.
[16] W. Neustock, A. Guarnieri, J. Demaison, G. Wlodarzak, Z. Naturforsch. A: Phys. Sci. 45 (1990) 702.
[17] P. Groner, S. Albert, E. Herbst, F. C. de Lucia, Astrophys. J. 500 (1998) 1059–1063.
[18] P. Groner, J. Chem. Phys. 107 (1997) 4483–4498.
[19] L. H. Coudert, P. Carcabal, M. Chevalier, M. Broquier, M. Hepp, M. Herman, J. Mol. Spectrosc. 212 (2002) 203–.
[20] Y. Niide, M. Hayashi, J. Mol. Spectr. 220 (2003) 65.
[21] C. P. Endres, B. J. Drouin, J. C. Pearson, H. S. P. Müller, F. Lewen, S. Schlemmer, T. F. Giesen, Astron. Astrophys. 504 (2009) 635–640.
[22] M. L. Senent, D. C. Moule, Y. G. Smeyers, Can. J. Phys. 73 (1995) 425–431.
[23] M. L. Senent, D. C. Moule, Y. G. Smeyers, J. Chem. Phys. 102 (1995) 5952–5959.
[24] M. Villa, M. L. Senent, R. Domínguez-Gómez, O. Álvarez-Bajo, M. Carvajal, J. Phys. Chem. A 115 (2011) 13573–13580.
[25] M. L. Senent, R. Domínguez-Gómez, M. Carvajal, M. Villa, J. Phys. Chem. A 116 (2012) 6901–6910.
[26] N. Ohashi, J. T. Hougen, R. D. Suenram, F. J. Lovas, Y. Kawashima, M. Fujitake, J. Pyka, J. Mol. Spectrosc. 227 (2004) 28–42.
[27] M. Tudorie, I. Kleiner, J. T. Hougen, S. Melandri, L. W. Sutikdja, W. Stahl, J. Mol. Spectrosc. 269 (2011) 211–225.
[28] K. Kobayashi, T. Matsui, N. Mori, S. Tsunekawa, N. Ohashi, J. Mol. Spectrosc. 269 (2011) 242–247.
[29] M. L. Senent, R. Ruiz, M. Villa, R. Domínguez-Gómez, J. Chem. Phys. 130 (2009) 064101 (10 pages).

[30] P. Schilke, D. J. Bendford, T. R. Hunter, D. C. Lis, T. G. Phillips, Astrophys. J. 132 (2001) 281.
[31] K. Demyk, G. Wlodarczak, M. Carvajal, A & A 489 (2008) 589–600.
[32] M. Koerber, S. Bisschop, C. Endres, F. Lewen, S. Schlemmer, Laboratory rotational spectrum of singly ^{13}c-substituted dimethyl ether up to 1.5 thz and interstellar detection of $^{13}ch_3o^{12}co_3$, in: J. Cernicharo, R. Bachiller (Eds.), Proceedings of IAU Symposium 280, Cambridge University Press, 2011, p. III.51.
[33] R. Lemus, Mol. Phys. 101 (2003) 2511–2528.
[34] O. Álvarez-Bajo, R. Lemus, M. Carvajal, F. Pérez-Bernal, Mol. Phys. 109 (2011) 797–812.
[35] G. E. Scuseria, H. F. Schaefer, III, J. Chem. Phys. 90 (1989) 3700.
[36] D. E. Woon, T. H. Dunning, Jr, J. Chem. Phys. 98 (1993) 1358.
[37] V. Szalay, A. G. Császár, M. L. Senent, J. Chem. Phys. 117 (2002) 6489.
[38] M. L. Senent, ENEDIM, *a variational code for non-rigid molecules*, 2001, in: FIT-ESPEC, *A Fortran code for calculating spectroscopic parameters from a force field in internal coordinates*, 2007, (see http://tct1.iem.csic.es/senent/PROGRAMAS.htm, for more details).
[39] M. L. Senent, Chem. Phys. Lett. 296 (1998) 299–306.
[40] W. Gordy, R. Cook, Microwave Molecular Spectra (3rd Edition), Knovel, 1984.
[41] I. Kleiner, J. Mol. Spectrosc. 260 (2010) 1–18.
[42] Y. G. Smeyers, M. N. Bellido, Int. J. Quant. Chem. 19 (1981) 553–565.
[43] P. R. Bunker, P. Jensen, Molecular Symmetry and Spectroscopy, NRC Research Press, Ottawa, 1989.
[44] J.-Q. Chen, Group Representation Theory for Physicists, World Scientific, 1989.

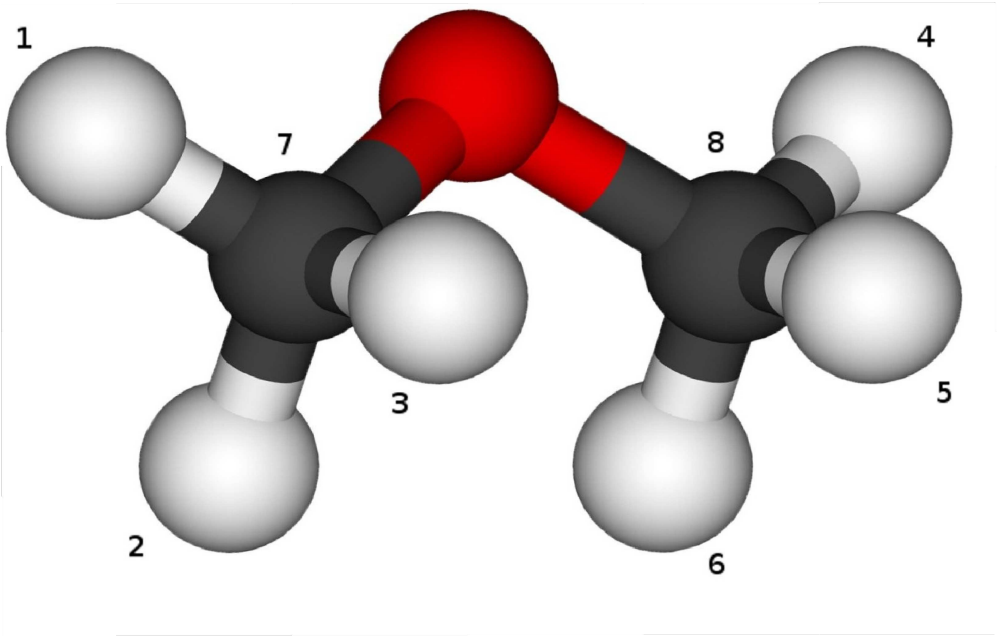

Figure 1. DME at the equilibrium structure and the numbering of nuclei considered in this work.

Table 1. Character table for the MS group $\mathcal{G}_{36}$ in terms of the group classes [43].

$\mathcal{G}_{36}$:	K_1	K_2	K_3	K_4	K_5	K_6	K_7	K_8	K_9
A_1	1	1	1	1	1	1	1	1	1
A_2	1	1	1	1	1	1	-1	-1	-1
A_3	1	1	-1	1	1	-1	1	1	-1
A_4	1	1	-1	1	1	-1	-1	-1	1
E_1	2	2	2	-1	-1	-1	0	0	0
E_2	2	2	-2	-1	-1	1	0	0	0
E_3	2	-1	0	2	-1	0	2	-1	0
E_4	2	-1	0	2	-1	0	-2	1	0
G	4	-2	0	-2	1	0	0	0	0

The $\mathcal{G}_{36}$ group classes are the following:

$$K_1 = \{E\} \; ; \quad K_2 = \{(123)(456), (132)(465)\} \; ; \quad K_3 = \{(14)(26)(35)(78)^*, (15)(24)(36)(78)^*, (16)(25)(34)(78)^*\}$$
$$K_4 = \{(123)(465), (132)(456)\} \; ; \quad K_5 = \{(123), (132), (456), (465)\}$$
$$K_6 = \{(142635)(78)^*, (143526)(78)^*, (162534)(78)^*, (153624)(78)^*, (163425)(78)^*, (152436)(78)^*\}$$
$$K_7 = \{(14)(25)(36)(78), (15)(26)(34)(78), (16)(24)(35)(78)\}$$
$$K_8 = \{(142536)(78), (143625)(78), (152634)(78), (163524)(78), (153426)(78), (162435)(78)\}$$
$$K_9 = \{(23)(56)^*, (13)(46)^*, (12)(45)^*, (23)(45)^*, (23)(46)^*, (13)(45)^*, (13)(56)^*, (12)(46)^*, (12)(56)^*\}$$

Table 2. Character Table for the MS group $C_{2v}(M)$.

$C_{2v}(M)$:	K'_1	K'_2	K'_3	K'_4
A_1	1	1	1	1
A_2	1	1	-1	-1
B_1	1	-1	-1	1
B_2	1	-1	1	-1

The $C_{2v}(M)$ group classes are the following:

$$K'_1 = E$$
$$K'_2 = (14)(25)(36)(78)$$
$$K'_3 = (23)(56)^*$$
$$K'_4 = (14)(26)(35)(78)^*$$

Table 3. Eigenvalues of the CSCO-II for a molecule with $\mathcal{G}_{36}$ symmetry.

$\mathcal{G}_{36}$	$C_{2v}(M)$	$\zeta = \nu + 2\mu$
A_1	A_1	20
A_2	B_1	-2
A_3	A_2	2
A_4	B_2	-20
E_1	A_1	11
E_1	B_1	7
E_2	A_2	-7
E_2	B_2	-11
E_3	A_1	17
E_3	A_2	5
E_4	B_1	-5
E_4	B_2	-17
G	A_1	8
G	A_2	-4
G	B_1	4
G	B_2	-8

Table 4. Eigenvectors of the CSCO-II for $\mathcal{G}_{36}$ from Eq. (11).

σ_a	σ_b	ζ	$Symm.^a$	$Eigenvector^b$
0	0	20	A_1, A_1	$\{1, 1, 1, 1\}$
		-2	A_2, B_1	$\{1, -1, -1, 1\}$
		2	A_3, A_2	$\{-1, -1, 1, 1\}$
		-20	A_4, B_2	$\{1, -1, 1, -1\}$
1	-1	11	E_1, A_1	$\{1, 1, 1, 1\}$
		7	E_1, B_1	$\{1, -1, -1, 1\}$
		-7	E_2, A_2	$\{-1, -1, 1, 1\}$
		-11	E_2, B_2	$\{-1, 1, -1, 1\}$
1	1	17	E_3, A_1	$\{1, 1, 1, 1\}$
		5	E_3, A_2	$\{-1, -1, 1, 1\}$
		-5	E_4, B_1	$\{1, -1, -1, 1\}$
		-17	E_4, B_2	$\{-1, 1, -1, 1\}$
1	0	8	G, A_1	$\{1, 1, 1, 1\}$
		-4	G, A_2	$\{-1, -1, 1, 1\}$
		4	G, B_1	$\{1, -1, -1, 1\}$
		-8	G, B_2	$\{-1, 1, -1, 1\}$

NOTES:
[a] The labels provide the irreducible representations of $\mathcal{G}_{36}$ and $C_{2v}(M)$ respectively, that means, the irreducible representations of $\mathcal{G}_{36}$ and their components.
[b] The four components of the eigenvectors refers to each 2D-torsional wavefunction of the subspace given in Eq. (11). The symmetry adapted basis will be obtained from a sum of the eigenvectors, with a given symmetry, for all possible values of k_a and k_b. The normalization should be considered too.

Table 5. Character table for the MS group $\mathcal{G}_{18}$ in terms of the group classes [26, 43].

$\mathcal{G}_{18}$	K_1	K_2	K_3	K_4	K_5	K_6
A_1	1	1	1	1	1	1
A_2	1	1	1	1	1	-1
E_1	2	2	-1	-1	-1	0
E_2	2	-1	2	-1	-1	0
E_3	2	-1	-1	2	-1	0
E_4	2	-1	-1	-1	2	0

The $\mathcal{G}_{18}$ group classes are the following:
$K_1 = E$; $K_2 = \{(456), (465)\}$; $K_3 = \{(123), (132)\}$; $K_4 = \{(123)(456), (132)(465)\}$; $K_5 = \{(123)(465), (132)(456)\}$;
$K_6 = \{(23)(56)^*, (13)(46)^*, (12)(45)^*, (23)(45)^*, (23)(46)^*, (13)(45)^*, (13)(56)^*, (12)(46)^*, (12)(56)^*\}$

Table 6. Subduction Table from the MS group $\mathcal{G}_{36}$ to $\mathcal{G}_{18}$.

(σ_a, σ_b)	$\mathcal{G}_{36}$	$\mathcal{G}_{36} \downarrow \mathcal{G}_{18}$
$(0, 0)$	A_1	A_1
	A_2	A_2
	A_3	A_2
	A_4	A_1
$(\pm1, \mp1)$	E_1	E_3
	E_2	E_3
$(\pm1, \pm1)$	E_3	E_4
	E_4	E_4
$(\pm1, 0)$,$(0, \pm1)$	G	$E_1 \oplus E_2$

NOTE: E_1 symmetry corresponds to $(\sigma_a, \sigma_b) = (\pm1, 0)$ and E_2 to $(\sigma_a, \sigma_b) = (0, \pm1)$.

Table 7. Subduction Table from the MS group $\mathcal{G}_{18}$ to $C_s(M)$.

(σ_a, σ_b)	$\mathcal{G}_{18}$	$\mathcal{G}_{18} \downarrow C_s(M)$
$(0, 0)$	A_1	A'
	A_2	A''
$(\pm1, 0)$	E_1	$A' \oplus A''$
$(0, \pm1)$	E_2	$A' \oplus A''$
$(\pm1, \mp1)$	E_3	$A' \oplus A''$
$(\pm1, \pm1)$	E_4	$A' \oplus A''$

Table 8. Character table for the MS group $C_s(M)$ [43].

$C_s(M)$	E	$(23)(56)^*$
A'	1	1
A''	1	-1

Table 9. *Ab initio* parameters of the adjusted effective torsional-bending potential (13).

Parameter	Value[a]	Parameter	Value[a]
A_{000}	970.9887	A_{220}	−0.1071
A_{100}	−54.7897	A_{202}	−0.1071
A_{200}	10.1393	A_{320}	0.0038
A_{300}	−0.1402	A_{302}	0.0038
A_{010}	−497.1729	A_{021}	0.8149
A_{001}	−497.1729	A_{012}	0.8149
A_{110}	31.7310	A_{121}	−0.3289
A_{101}	31.7310	A_{112}	−0.3289
A_{210}	−1.0805	A_{221}	0.0481
A_{201}	−1.0805	A_{212}	0.0481
A_{310}	0.0134	A_{321}	0.0026
A_{301}	0.0134	A_{312}	0.0026
A_{011}	26.7661	A_{022}	1.3639
A_{111}	−12.7102	A_{122}	−0.0958
A_{211}	0.5208	A_{222}	−0.0293
A_{311}	−0.0056	A_{322}	0.0026
A_{020}	−3.2897	B_{011}	−2.8995
A_{002}	−3.2897	B_{111}	14.3670
A_{120}	1.1183	B_{211}	−0.7375
A_{102}	1.1183	B_{311}	0.0117

[a] The parameter values are expressed in cm^{-1} and degrees.

Table 10. *Ab initio* parameters[a] of the adjusted 3D torsional-bending Kinetic operator (14).

Parameter[b]	Value[c]	Parameter[b]	Value[c]	Parameter[b]	Value[c]
C_{aa}^{000}	6.7378	C_{bb}^{000}	6.7169	C_{ab}^{000}	−1.2002
C_{aa}^{100}	0.0451	C_{bb}^{100}	0.0451	C_{ab}^{100}	−0.0543
C_{aa}^{200}	0.0012	C_{bb}^{200}	0.0012	C_{ab}^{200}	−0.0010
C_{aa}^{010}	−0.0089	C_{bb}^{010}	0.0013	C_{ab}^{010}	−0.0102
C_{aa}^{001}	0.0014	C_{bb}^{001}	−0.0089	C_{ab}^{001}	−0.0102
C_{aa}^{110}	0.0021	C_{bb}^{101}	0.0021	C_{ab}^{020}	0.0022
C_{aa}^{011}	0.0036	C_{bb}^{011}	0.0036	C_{ab}^{002}	0.0023
C_{aa}^{002}	−0.0016	C_{bb}^{020}	−0.0015		
S_{aa}^{011}	−0.0023	S_{bb}^{011}	−0.0023		
$C_{\alpha\alpha}^{000}$	5170.2152	$C_{\alpha\alpha}^{100}$	55.3450	$C_{\alpha\alpha}^{200}$	0.0180
$C_{\alpha\alpha}^{300}$	−0.0081				

[a] Only the parameters with values higher than 10^{-3} are shown.
[b] The subindexes *a* and *b* of the kinetic matrix elements stand for the internal torsional coordinates θ_1 and θ_2 respectively.
[c] The parameter values are expressed in cm^{-1} and degrees.

Table 11: Calculated Infrared transitions given by a CCSD(T) potential.

v_t	v'_t	n_b	Symm.		v_t	v'_t	n_b	Symm.	CCSD(T)[a]	Adjusted[b]
1	0	0	A_2	←	0	0	0	A_1	198.453	200.912
1	0	0	E_1	←	0	0	0	E_1	198.444	200.903
1	0	0	E_2	←	0	0	0	E_2	198.444	200.904
1	0	0	E_3	←	0	0	0	E_3	198.435	200.894
1	0	0	E_4	←	0	0	0	E_4	198.435	200.894
0	1	0	A_2	←	0	0	0	A_1	244.553	241.607
0	1	0	E_1	←	0	0	0	E_1	244.544	241.598
0	1	0	E_2	←	0	0	0	E_2	244.544	241.598
0	1	0	E_3	←	0	0	0	E_3	244.534	241.588
0	1	0	E_4	←	0	0	0	E_4	244.534	241.588
2	0	0	A_1	←	0	1	0	A_2	142.567	148.002
2	0	0	E_1	←	0	1	0	E_1	142.702	148.134
2	0	0	E_2	←	0	1	0	E_2	142.704	148.136
2	0	0	E_3	←	0	1	0	E_3	142.841	148.270
2	0	0	E_4	←	0	1	0	E_4	142.841	148.270
2	0	0	A_1	←	1	0	0	A_2	188.667	188.697
2	0	0	E_1	←	1	0	0	E_1	188.802	188.829
2	0	0	E_2	←	1	0	0	E_2	188.804	188.830
2	0	0	E_3	←	1	0	0	E_3	188.940	188.964
2	0	0	E_4	←	1	0	0	E_4	188.940	188.964
0	2	0	A_1	←	0	1	0	A_2	241.537	238.380
0	2	0	E_1	←	0	1	0	E_1	241.626	238.461
0	2	0	E_2	←	0	1	0	E_2	241.624	238.459
0	2	0	E_3	←	0	1	0	E_3	241.713	238.540
0	2	0	E_4	←	0	1	0	E_4	241.712	238.540
0	2	0	A_1	←	1	0	0	A_2	287.637	279.075
0	2	0	E_1	←	1	0	0	E_1	287.726	279.156
0	2	0	E_2	←	1	0	0	E_2	287.724	279.153
0	2	0	E_3	←	1	0	0	E_3	287.812	279.234
0	2	0	E_4	←	1	0	0	E_4	287.811	279.234
1	1	0	A_1	←	0	1	0	A_2	177.520	180.022
1	1	0	E_1	←	0	1	0	E_1	177.749	180.248
1	1	0	E_2	←	0	1	0	E_2	177.742	180.240
1	1	0	E_3	←	0	1	0	E_3	177.970	180.464
1	1	0	E_4	←	0	1	0	E_4	177.970	180.465
1	1	0	A_1	←	1	0	0	A_2	223.620	220.717
1	1	0	E_1	←	1	0	0	E_1	223.849	220.943
1	1	0	E_2	←	1	0	0	E_2	223.842	220.934
1	1	0	E_3	←	1	0	0	E_3	224.069	221.158
1	1	0	E_4	←	1	0	0	E_4	224.069	221.159

Table 11 – Continuation.

v_t	v'_t	n_b	Symm.		v_t	v'_t	n_b	Symm.	CCSD(T)[a]	Adjusted[b]
2	1	0	A_2	←	2	0	0	A_1	202.118	200.287
2	1	0	E_1	←	2	0	0	E_1	199.654	197.852
2	1	0	E_2	←	2	0	0	E_2	199.755	197.969
2	1	0	E_3	←	2	0	0	E_3	197.111	195.293
2	1	0	E_4	←	2	0	0	E_4	197.112	195.294
1	2	0	A_2	←	1	1	0	A_1	229.572	225.090
1	2	0	E_1	←	1	1	0	E_1	228.109	223.681
1	2	0	E_2	←	1	1	0	E_2	228.150	223.726
1	2	0	E_3	←	1	1	0	E_3	226.657	222.275
1	2	0	E_4	←	1	1	0	E_4	226.645	222.265
1	0	1	A_2	←	0	0	1	A_1	196.493	201.032
1	0	1	E_1	←	0	0	1	E_1	196.489	201.117
1	0	1	E_2	←	0	0	1	E_2	196.495	201.118
1	0	1	E_3	←	0	0	1	E_3	196.475	201.203
1	0	1	E_4	←	0	0	1	E_4	196.474	201.202
0	1	1	A_2	←	0	0	1	A_1	226.544	224.874
0	1	1	E_1	←	0	0	1	E_1	226.605	224.922
0	1	1	E_2	←	0	0	1	E_2	226.603	224.917
0	1	1	E_3	←	0	0	1	E_3	226.664	224.968
0	1	1	E_4	←	0	0	1	E_4	226.665	224.968

[a] CCSD(T)/aug-cc-pVTZ

[b] Adjusted Hamiltonian given in Ref. [24] after including the corrections derived from the definition of α coordinate and the isotopic structural changes.

Table 12. Calculated Raman transitions given by a CCSD(T) potential.

v_t	v_t'	n_b	Symm.		v_t	v_t'	n_b	Symm.	CCSD(T)[a]	Adjusted[b]
0	0	1	A_1	←	0	0	0	A_1	418.537	409.170
0	0	1	E_1	←	0	0	0	E_1	418.534	409.173
0	0	1	E_2	←	0	0	0	E_2	418.534	409.173
0	0	1	E_3	←	0	0	0	E_3	418.530	409.175
0	0	1	E_4	←	0	0	0	E_4	418.530	409.175
2	0	0	A_1	←	0	0	0	A_1	387.120	389.609
2	0	0	E_1	←	0	0	0	E_1	387.246	389.732
2	0	0	E_2	←	0	0	0	E_2	387.248	389.734
2	0	0	E_3	←	0	0	0	E_3	387.375	389.858
2	0	0	E_4	←	0	0	0	E_4	387.375	389.858
1	1	0	A_1	←	0	0	0	A_1	422.073	421.629
1	1	0	E_1	←	0	0	0	E_1	422.293	421.846
1	1	0	E_2	←	0	0	0	E_2	422.286	421.838
1	1	0	E_3	←	0	0	0	E_3	422.504	422.052
1	1	0	E_4	←	0	0	0	E_4	422.504	422.053
0	2	0	A_1	←	0	0	0	A_1	486.090	479.987
0	2	0	E_1	←	0	0	0	E_1	486.170	480.059
0	2	0	E_2	←	0	0	0	E_2	486.168	480.057
0	2	0	E_3	←	0	0	0	E_3	486.247	480.128
0	2	0	E_4	←	0	0	0	E_4	486.246	480.128
1	2	0	A_2	←	1	0	0	A_2	453.192	445.807
1	2	0	E_1	←	1	0	0	E_1	451.958	444.624
1	2	0	E_2	←	1	0	0	E_2	451.992	444.660
1	2	0	E_3	←	1	0	0	E_3	450.726	443.433
1	2	0	E_4	←	1	0	0	E_4	450.714	443.424

[a] CCSD(T)/aug-cc-pVTZ

[b] Adjusted Hamiltonian given in Ref. [24] after including the corrections derived from the definition of α coordinate and the isotopic structural changes.